Applied Catalysis B: Environmental 207 (2017) 60–71

Contents lists available at ScienceDirect

Applied Catalysis B: Environmental

journal homepage: www.elsevier.com/locate/apcatb

An alumina-supported silver catalyst with high water tolerance for H_2 assisted C_3H_6-SCR of NOx

Guangyan Xu[a,b,1], Jinzhu Ma[a,b,c,1], Guangzhi He[a], Yunbo Yu[a,b,c,*], Hong He[a,b,c,*]

[a] State key Joint Laboratory of Environment Simulation and Pollution Control, Research Center for Eco-Environmental Sciences, Chinese Academy of Sciences, Beijing 100085, China
[b] University of Chinese Academy of Sciences, Beijing 100049, China
[c] Center for Excellence in Regional Atmospheric Environment, Institute of Urban Environment, Chinese Academy of Sciences, Xiamen 361021, China

ARTICLE INFO

Article history:
Received 11 November 2016
Received in revised form 20 January 2017
Accepted 1 February 2017
Available online 1 February 2017

Keywords:
Ag/Al_2O_3
HC-SCR
Water vapor
H_2
DFT

ABSTRACT

Water vapor is typically present in diesel engine exhausts, and thus the design of catalysts with high water-tolerance is highly desired. The addition of water vapor was shown to have quite different influences on the activity of Ag/Al_2O_3 catalysts with different Ag loadings during the H_2-assisted C_3H_6-SCR of NOx (H_2-C_3H_6-SCR). The 2 wt% Ag/Al_2O_3 catalyst showed the best activity for H_2-C_3H_6-SCR, with excellent water resistance over the whole temperature range. An enhancement in NOx conversion was observed after water vapor was introduced, particularly at low temperatures. Over this catalyst, kinetic studies confirmed that H_2O addition did not change the apparent activation energy for NOx reduction, while it increased the reaction order of C_3H_6 from −0.62 to 0.73. This result indicated that the reaction pathway for NOx reduction was hardly changed by the introduction of water vapor, while a poisoning effect related to C_3H_6 oxidation was decreased. *In situ* DRIFTS studies and DFT calculations revealed that water vapor significantly inhibits the formation of inert formate during the H_2-C_3H_6-SCR process, and thus more sites are available for the formation of active enolic species and acetates, finally leading to increased activity for 2 wt% Ag/Al_2O_3 in NOx reduction.

© 2017 Elsevier B.V. All rights reserved.

1. Introduction

Nitrogen oxides (NO_x), as key precursors to pollutants, induce the formation of acid rain, photochemical smog, and haze. Nowadays, diesel engine NOx after-treatment is one of the greatest challenges in environmental protection. To this aim, different technologies have been developed, among which selective catalytic reduction by hydrocarbons (HC-SCR) has been paid much attention in the past few decades, considering that the on-board diesel or a fuel additive can be used as the reducing agent for NOx removal, thus providing an opportunity for simplification of the after-treatment system [1–4]. Previous studies have proved that Ag/Al_2O_3 is one of the most promising catalysts for NOx reduction by hydrocarbons [1–3,5–10]. At low temperatures, however, the activity of Ag/Al_2O_3 for HC-SCR is not sufficient for its commercial usage in purification of diesel vehicle exhausts.

The discovery of a promoting effect of hydrogen on the low-temperature activity of Ag/Al_2O_3 catalysts by Satokawa et al. [11,12] is undoubtedly a major breakthrough for HC-SCR. Since then, many efforts have been devoted to understanding the "H_2 effect" occurring during NOx reduction by lighter hydrocarbons [13–17], higher hydrocarbons [18,19] and alcohols [20] over silver catalysts. At present, the origin of H_2 boosting behavior on the low-temperature activity of Ag/Al_2O_3 for NOx reduction by hydrocarbons has not been revealed in full detail, while it is clear that the presence of H_2 enhances the transformation of hydrocarbons to partially oxidized species. These oxygenates have been proved to be active intermediates for NOx reduction, leading to an increase in the NOx conversion at low temperatures [15,21–23].

Water vapor is inevitably present in diesel engine exhausts and thus the design of catalysts with high water tolerance is highly desired. However, the influence of water vapor on HC-SCR processes has attracted a limited number of investigations [24–26]. The water tolerance of the 2 wt% Ag/Al_2O_3 catalyst for NOx reduction by different alkanes was studied by Shimizu et al. [24]. It was found that the activity of Ag/Al_2O_3 for NOx reduction and its water resistance were gradually increased with an increase in the carbon number of alkanes. In the case of *n*-octane as a reductant, a signif-

* Corresponding authors at: State key Joint Laboratory of Environment Simulation and Pollution Control, Research Center for Eco-Environmental Sciences, Chinese Academy of Sciences, Beijing 100085, China.
E-mail addresses: ybyu@rcees.ac.cn (Y. Yu), honghe@rcees.ac.cn (H. He).
[1] These authors contributed equally.

http://dx.doi.org/10.1016/j.apcatb.2017.02.001
0926-3373/© 2017 Elsevier B.V. All rights reserved.

icant promotion effect on NOx conversion was induced by water vapor addition, the occurrence of which possibly related to an inhibition of the unselective oxidation of *n*-octane and a suppression of poisoning by carboxylate and carbonate species. Over 1.2 wt% Ag/Al_2O_3, a significant loss in NOx conversion induced by the presence of H_2O was observed by Meunier et al. [25] during C_3H_6-SCR. As for C_3H_8-SCR and H_2-C_3H_8-SCR over 5 wt% Ag/Al_2O_3, decreased NOx conversion was also observed in the presence of water vapor [27].

It is well-known that silver loading has a great influence on the activity of Ag/Al_2O_3 catalysts for NOx reduction by hydrocarbons [28–30], and also for H_2-assisted HC-SCR processes [31–33]. To the best of our knowledge, however, there has been no study focusing on the effect of silver loading on the water tolerance of Ag/Al_2O_3 for H_2-assisted HC-SCR. Herein, it was found that silver loading governs the water tolerance of Ag/Al_2O_3 for H_2-C_3H_6-SCR. Based on a kinetic study and *in situ* DRIFTS measurements, the origin of the water vapor effect on the pathway of H_2-C_3H_6-SCR was revealed. This investigation could offer new insights into the design of silver catalysts for HC-SCR with high water resistance.

2. Materials and methods

2.1. Catalyst preparation and characterization

A series of Ag/Al_2O_3 catalysts with varying Ag loadings (1, 2, 4, and 6 wt%) were synthesized by an impregnation method, with boehmite (SASOL, SB-1) and silver nitrate as the precursors. The detailed information can be found in our previous studies [2,34]. All the samples presented here were calcined in air at 600 °C for 3 h. A pure Al_2O_3 sample was also prepared by the same procedure, with boehmite as the precursor.

The BET surface area measurements were carried out on a Quantachrome Autosorb-1C instrument at −196 °C. X-ray powder diffraction patterns were measured on a Rigaku D/max-RB X-ray Diffractometer (Japan) with Cu Kα radiation (over the 2θ range from 10° to 80°).

UV-vis spectra were collected with a UV–vis spectrophotometer (Hitachi, U3100, Japan) within a range of 200–800 nm with a resolution of 5 nm, using Al_2O_3 as reference to confirm the baseline spectrum. XANES analyses of the Ag-K edges were performed in transmission mode at the BL14W1 XAFS beam line at the Shanghai Synchrotron Radiation Facility (SSRF). The PE storage ring was operated at 3.5 GeV with 200 mA as the average storage current. Data were analyzed using the Athena program.

2.2. Catalyst activity studies

The catalytic measurements were performed in a fixed-bed reactor, by stepwise increase of the temperature and measurement after 30 min reaction at each temperature [35,36]. The feed composition included 800 ppm NO, 1714 ppm C_3H_6, 1% H_2 (if added), 10% O_2, 10% H_2O (if added) in N_2 balance at a total flow of 1000 ml/min, corresponding to a gas hourly space velocity (GHSV) of 100,000 h^{-1} (ca 0.3 g catalyst). The concentrations of NO, NO_2, NH_3, N_2O, and C_3H_6 were measured by an FTIR spectrometer (Nicolet Nexus is10). Water vapor was supplied into the gas stream with a micropump and further vaporized by an electric heater. To avoid water condensation, the gas-filled tube and the gas cell of the FTIR spectrophotometer were heated to 120 °C. NOx conversion and C_3H_6 conversion were calculated as shown in the following equations, respectively:

$$NOx\ conversion = \frac{[NO]_{in} + [NO_2]_{in} - [NO]_{out} - [NO_2]_{out}}{[NO]_{in} + [NO_2]_{in}} \times 100\% \quad (1)$$

$$C_3H_6\ conversion = \frac{[C_3H_6]_{in} - [C_3H_6]_{out}}{[C_3H_6]_{in}} \times 100\% \quad (2)$$

2.3. Kinetic studies

The apparent activation energy (Ea) and reaction order for NOx reduction were measured in the fixed-bed reactor as described above. To eliminate both internal diffusion and external mass transfer resistances, corresponding experiments were performed with results shown in Fig. S1 and Supplementary material. Based on these results, samples with a particle size of 0.45–0.9 mm were used for kinetic measurement. The value of GHSV was varied in the range of 100,000–3,000,000 h^{-1} in order to keep NOx conversion below 20%. Before kinetic measurements, all samples were pretreated in 10% O_2/N_2 at 450 °C for 30 min.

In agreement with previous studies [35,37], the reaction rate of NOx conversion ($-R_{NOx}$) can be calculated from the kinetic data as follows:

$$-R_{NOx}\left(mol/m^2/s\right) = F_{NOx} \times X_{NOx}/(W \times S) \quad (3)$$

where F_{NOx} is the molar flow rate of NOx (mol/s), X_{NOx} is the conversion of NOx, W is the weight of catalyst, and S is the BET surface area. Based on the above results, the Arrhenius plots for NOx reduction under different conditions were drawn, and then the related activation energies were calculated from the slope of the plots.

2.4. In situ *DRIFTS studies*

In situ DRIFTS experiments were performed on a Nicolet Nexus FI-IR spectrometer (Nexus 670) with 30 scans at a resolution of 4 cm^{-1}, under a total gas flow rate of 300 ml/min. Water vapor (5%) was supplied by passing the gas flow through a water bottle, with the gas line heated to 120 °C to avoid water condensation. Before each measurement, the Ag/Al_2O_3 catalysts were pretreated in 10% O_2/N_2 at 350 °C for 0.5 h, which was followed by cooling down to the desired temperature to measure a background spectrum.

2.5. DFT calculations

All DFT calculations were carried out by use of the CASTEP package from Accelrys. The Perdew–Wang (PW91) functional of the generalized gradient approximation (GGA) was used as the exchange–correlation function. Convergence tests were done for all initial parameters. The interaction between valence electrons and the ionic core was described by an ultrasoft pseudopotential. The vacuum gap was 20 Å to avoid inter-slab interactions in the periodic systems. Calculations were carried out with a plane-wave energy cutoff of 400 eV. Based on our previous reports [38,39], the dehydrated (100) and (110) surfaces of γ-Al_2O_3 were modeled using a (2 × 2) supercells and four-layer-thick slabs, $Al_{80}O_{120}$ with surface area of 11.17 × 16.83 $Å^2$ and $Al_{64}O_{96}$ with surface area of 16.83 × 16.14 $Å^2$, respectively. For the Ag/Al_2O_3 (100) surface (Ag–O–Al_{octa} entities) and Ag/Al_2O_3 (110) surface (Ag–O–Al_{tetra} entities), the AgO units adsorbed on the Al_2O_3 surfaces mentioned above were established and relaxed (Fig. S2) [38]. To investigate the effect of H_2O on the adsorption of the adsorbates, the Ag/Al_2O_3 surfaces were hydroxylated. The 12OH-Ag/Al_2O_3 (100) surface and 20OH-Ag/Al_2O_3 (110) surface were established according to previous calculations [40], and the coverage of hydroxyl was calculated to be 6.4 OH nm^{-2} and 7.4 OH nm^{-2}, respectively. According to our earlier convergence test, the Monkhorst–Pack k-point sets of (2 × 1 × 1) and (1 × 1 × 1) were used for the Al_2O_3 (100) and Al_2O_3 (110) surfaces, respectively [38]. The top two layers and the adsorbents were fully relaxed, while the bottom two layers were fixed to mimic the bulk region. The relaxed structures of the hydroxylated Ag/Al_2O_3 slabs are shown in Fig. S3.

Table 1
Structure parameters of Ag/Al_2O_3 catalysts with different silver loadings.

Sample	BET surface area (m^2/g)	Pore volume (cm^3/g)	Pore diameter (nm)
γ-Al_2O_3	271.2	0.59	10.33
1 wt% Ag/Al_2O_3	222.5	0.56	10.13
2 wt% Ag/Al_2O_3	220.8	0.55	9.91
4 wt% Ag/Al_2O_3	220.6	0.51	9.33
6 wt% Ag/Al_2O_3	214.7	0.48	8.99

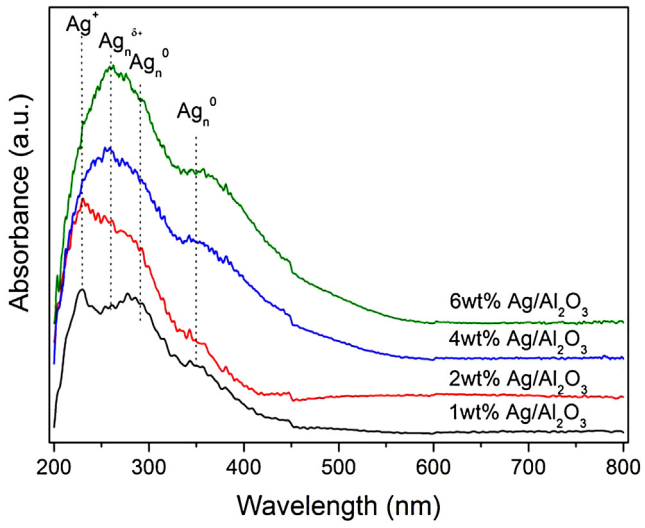

Fig 1. The UV–vis spectra of Ag/Al_2O_3 catalysts with different silver loadings.

The adsorption energies of the intermediates produced by partial oxidation of C_3H_6 ($HCOO^-$, $CH_2{=}CHO^-$, and CH_3COO^-) on the Ag/Al_2O_3 surface or the hydroxylated one were calculated as follows:

$$E_{ad} = E_{adsorbate+surface} - (E_{surface} + E_{adsorbate}),$$

where $E_{adsorbate+surface}$ and $E_{surface}$ are the total energies of the adsorbed system and alumina slab, respectively; and E_{ad} reflects the stability of the adsorbates on either the Ag/Al_2O_3 or the hydroxylated Ag/Al_2O_3 surface. Negative E_{ad} values mean that the adsorbed state is energetically favorable.

3. Results

3.1. Structural properties of Ag/Al_2O_3 catalysts

As shown in Table 1, the Al_2O_3 exhibited a BET surface area of 271.2 m^2/g. Compared with the pure Al_2O_3, the Ag/Al_2O_3 catalysts showed a decrease in surface area, particularly the catalysts with high silver loading [34,35,41]. XRD patterns showed that only the γ-Al_2O_3 phase was detected in all Ag/Al_2O_3 catalysts, indicating that Ag was dispersed well on the Al_2O_3 (Fig. S4).

To investigate the state of silver supported on Al_2O_3, UV–vis analysis was performed, with results shown in Fig. 1. According to the literature [4,18,42], the band located at 230 nm is attributed to silver cations (Ag^+) with high dispersion. The appearance of the peak at 260 nm indicates that oxidized silver clusters ($Ag_n^{\delta+}$) are present on the surface of Ag/Al_2O_3. In addition, peaks appearing at 290 and 350 nm can be assigned to metallic silver clusters (Ag_n^0). On the 1 wt% and 2 wt% Ag/Al_2O_3, notably, the band at 230 nm exhibited the highest intensity, indicating that highly dispersed silver ions were predominant. As for the samples with 4 wt% and 6 wt% silver loadings, however, the intensity of the band at 260 nm was the highest, suggesting that the silver species were mainly present as oxidized silver clusters. For these two samples, meanwhile, strong peaks at 350 nm were clearly observed, indicating the existence of numerous metallic silver clusters [2,34,35].

To better understand the precise chemical state of supported silver, the Ag-K XANES spectra of samples with different silver loadings, Ag foil, and $AgNO_3$ were investigated (Fig. S5). As shown in Fig. S5A, the Ag/Al_2O_3 catalysts showed Ag-K adsorption edge energies similar to that of $AgNO_3$, while being higher than that of Ag foil. The first-order derivative peak for 2 wt%, 4 wt%, 6 wt% Ag/Al_2O_3 catalysts and $AgNO_3$ appeared at 25517.5 eV, 25516.4 eV, 25516.7 eV, and 25518.6 eV, respectively. In contrast, the corresponding absorption edge energy for the Ag-K edge in Ag foil was 25514.4 eV (Fig. S5B). These findings further confirm that silver species were mainly present as oxidized silver on 2 wt% Ag/Al_2O_3, while the silver species exhibited a partially metallic state on 4 wt% and 6 wt% Ag/Al_2O_3 [34].

3.2. Effect of H_2O on the deNOx activity of Ag/Al_2O_3

Fig. 2 shows that the low-temperature activity of Ag/Al_2O_3 for C_3H_6-SCR can be promoted greatly by H_2 introduction. In the absence of water vapor, it should be noted that the higher the silver loading, the better the low-temperature activity of Ag/Al_2O_3 for H_2-assisted C_3H_6-SCR (denoted as H_2-C_3H_6-SCR) is. During this H_2-C_3H_6-SCR process, however, water vapor exhibits quite a different influence on NOx conversion, which is also closely related to the silver loading. Over 1 wt% Ag/Al_2O_3, water vapor had little influence on H_2-C_3H_6-SCR at temperatures below 420 °C, while further increasing the reaction temperature (>420 °C) significantly lowered the NOx conversion. In the presence of H_2, the catalyst with 2 wt% silver loading exhibited excellent activity for NOx conversion, achieving 100% NOx conversion over a wide temperature range of 295–530 °C. What is more, this catalyst exhibited high water resistance, particularly at low temperatures. Over this sample, indeed, one can easily find an enhancement of NOx conversion at temperatures below 300 °C. Compared with 2 wt% Ag/Al_2O_3, the samples with silver loadings of 4 wt% and 6 wt% showed better low-temperature activity for NOx reduction in the presence of H_2. However, their activity was severely suppressed by the introduction of water vapor over the whole temperature range. In the presence of water vapor, the 2 wt% Ag/Al_2O_3 clearly exhibited the highest activity for H_2-C_3H_6-SCR, indicating excellent water resistance.

During the H_2-C_3H_6-SCR process, C_3H_6 conversion was also measured, with results shown in Fig. 3. At temperatures below 400 °C, the activity of 1 wt% Ag/Al_2O_3 for C_3H_6 conversion was hardly changed by water introduction, while at high temperatures, C_3H_6 conversion obviously decreased with the addition of water vapor. Over the 2 wt% Ag/Al_2O_3, the C_3H_6 conversion at low temperatures was enhanced by the introduction of H_2O. As for the 4 wt% and 6 wt% Ag/Al_2O_3 samples, the presence of water vapor severely suppressed C_3H_6 conversion in the whole temperature range.

Combining the results of Figs. 2 and 3, one can easily find that over a given sample, the changes in NOx and C_3H_6 conversion exhibit the same trend when water vapor is introduced, indicating that C_3H_6 oxidation plays a crucial role in the reduction of NOx. To further confirm such influence of water vapor on H_2-assisted C_3H_6-SCR, a series of step-response experiments were carried out over Ag/Al_2O_3, at the temperatures of 265 °C and 400 °C, respectively (Figs. 4 and S6). In these cases, the weight of sample employed was varied in the range of 0.1–0.4 g in order to keep NOx conversion below 90%. Over the sample with 2 wt% silver loading, the NOx conversion at 265 °C was increased from 22% to 38% by the introduction of water vapor, while it returned to 20% after the removal of water vapor (Fig. 4A). During this process, meanwhile, the C_3H_6 conversion showed the same trend as the NOx conversion, further

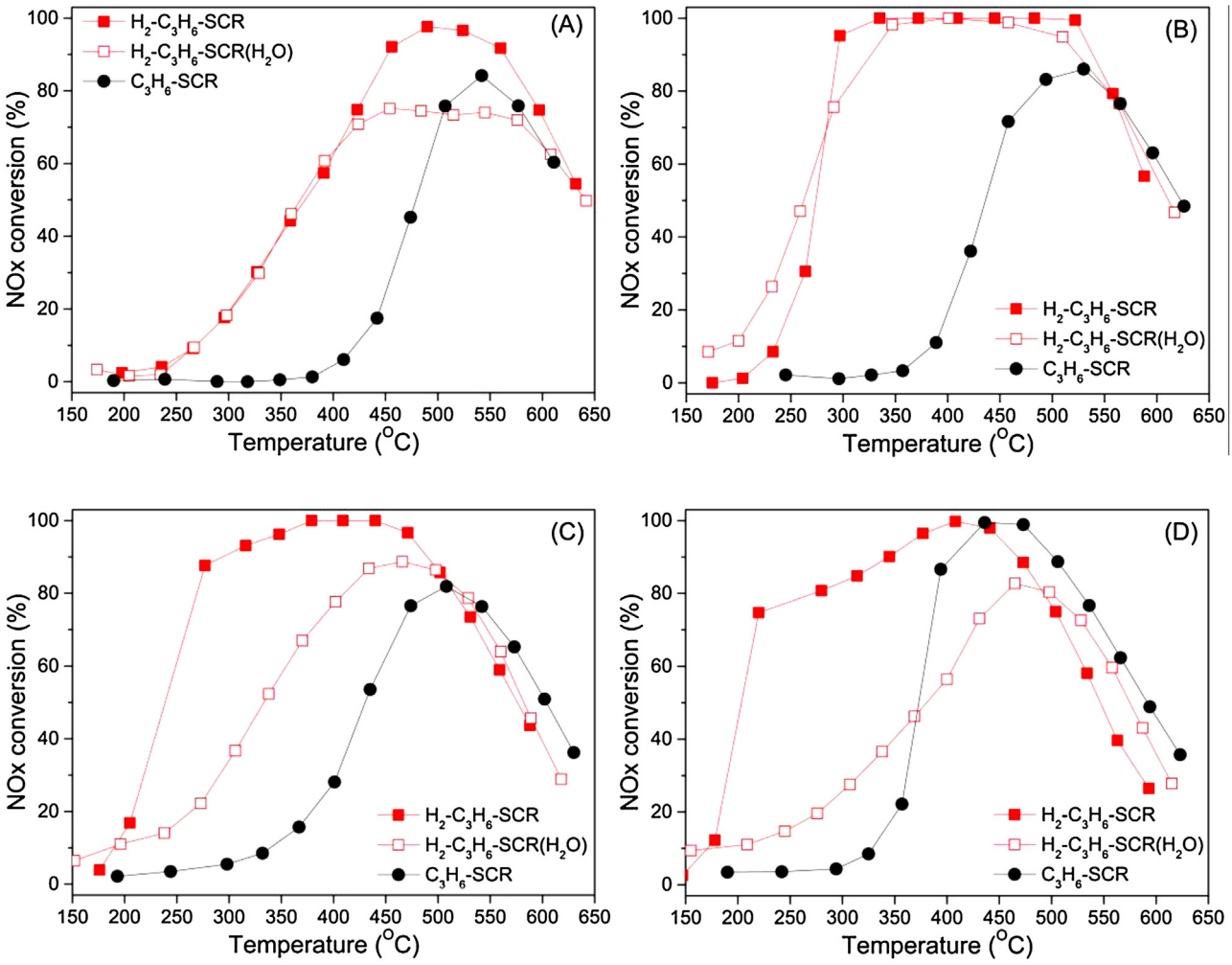

Fig. 2. NOx conversions over (A) 1 wt% Ag/Al_2O_3, (B) 2 wt% Ag/Al_2O_3, (C) 4 wt% Ag/Al_2O_3, and (D) 6 wt% Ag/Al_2O_3 under different conditions: H_2-C_3H_6-SCR (■), H_2-C_3H_6-SCR with H_2O (□), and C_3H_6-SCR (●). Feed composition: 800 ppm NO, 1714 ppm C_3H_6, 1% H_2 (when added), 10% H_2O (when added), 10% O_2, N_2 balance. GHSV: 100,000 h^{-1}.

confirming a crucial role of C_3H_6 partial oxidation in the reduction of NOx. At the same reaction temperature, however, the activity of 4 wt% Ag/Al_2O_3 was suppressed severely by water vapor addition (from 74% to 27%), accompanied by a significant loss in C_3H_6 conversion (Fig. 4B). After the removal of water vapor, again, both the NOx and C_3H_6 conversion was restored to the original levels. Even at the temperature of 400 °C, the activity of 2 wt% Ag/Al_2O_3 for NOx and C_3H_6 conversion was hardly affected by the addition of water vapor (Fig. 4C), further confirming its excellent water tolerance. As shown in Fig. S6, the performance of 1 wt% Ag/Al_2O_3 for NOx and C_3H_6 conversion was slightly enhanced by the addition of water vapor, while the low-temperature activity of 6 wt% Ag/Al_2O_3 was severely suppressed (NOx conversion decreased from 55% to 15%).

3.3. *Kinetic studies of Ag/Al_2O_3 for H_2-C_3H_6-SCR*

3.3.1. *Apparent activation energy*

Kinetics has been shown to be extremely valuable in providing unique information on the understanding of catalytic reactions at a molecular level [43], and much attention has been paid to the kinetics of HC-SCR processes [13,24,27,29,31,35,37,41,44–55]. With this in mind, we also carried out kinetic experiments to gain further insights into the influence of water vapor in H_2-C_3H_6-SCR over Ag/Al_2O_3 catalysts.

Fig. 5 presents Arrhenius plots of the reaction rate for NOx conversion over Ag/Al_2O_3 samples with varying silver loadings. Based on these results, the apparent activation energies (Ea) for NOx conversion under the employed experimental conditions were calculated, with results listed in Table 2. Over all the Ag/Al_2O_3 samples, the Ea values for the H_2-C_3H_6-SCR varied from 49.9 to 66.1 kJ/mol (Fig. 5A and Table 2), consistent with the literature [13,31]. For a given sample, introduction of water vapor induced a slight decrease in the value of Ea (Fig. 5B and Table 2). The Ea for NOx reduction in the absence of H_2 was also measured over 2 wt% and 4 wt% Ag/Al_2O_3 (Fig. 5C). In this case, the presence of water vapor resulted in an increase of ca. 40 kJ/mol in the Ea value for NOx reduction. Therefore, it can be speculated that water vapor did not change the pathway of the H_2-assisted C_3H_6-SCR over Ag/Al_2O_3 catalysts. To further reveal the role of water vapor in H_2-C_3H_6-SCR, the following studies focused on the 2 wt% and 4 wt% Ag/Al_2O_3 catalysts.

3.3.2. *Reaction order for NOx reduction*

Fig. 6 and Table 3 show the dependence of the NOx conversion rate on the concentrations of NO and C_3H_6 over Ag/Al_2O_3 at 280 °C. Over 2 wt% Ag/Al_2O_3, the empirical reaction order of NO for NOx reduction in the presence of H_2 was 0.56. This result indicates a possibility that the reaction rate is substantially controlled by the surface reaction [1–3,5]. Over this catalyst, introduction of water

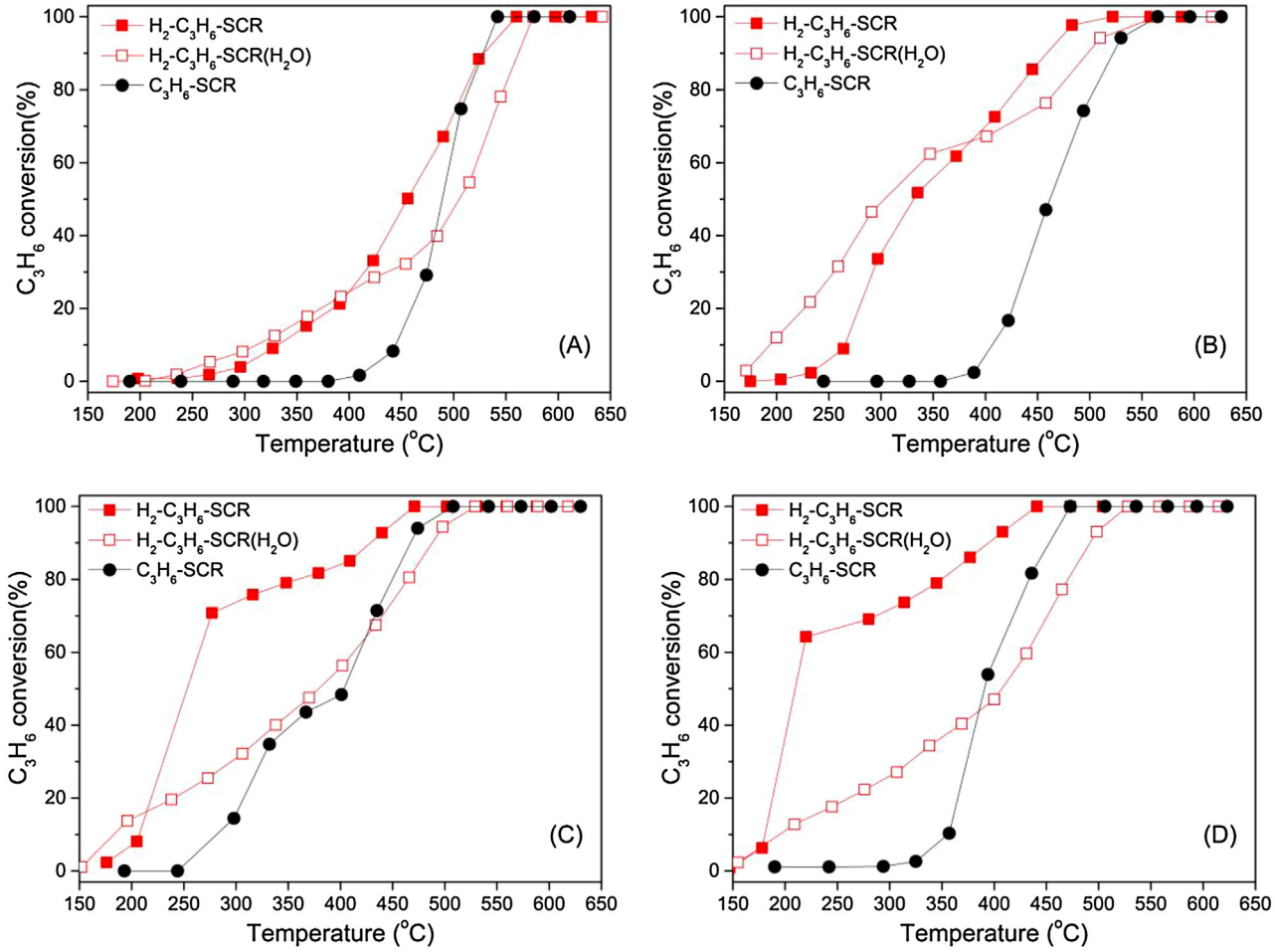

Fig. 3. C_3H_6 conversions over (A) 1 wt% Ag/Al_2O_3, (B) 2 wt% Ag/Al_2O_3, (C) 4 wt% Ag/Al_2O_3, and (D) 6 wt% Ag/Al_2O_3 under different conditions: H_2-C_3H_6-SCR (■), H_2-C_3H_6-SCR with water (□), and C_3H_6-SCR (●). The feed composition was the same as Fig. 2.

Table 2
Apparent activation energy (Ea) for NOx conversion over Ag/Al_2O_3.

Sample	Activation energy (kJ/mol)		Reductant	Ref.
	0% H_2O	10% H_2O		
1 wt% Ag/Al_2O_3	49.9	46.1	H_2+C_3H_6	This work
2 wt% Ag/Al_2O_3	62.3	60.2	H_2+C_3H_6	This work
	74.1	115.4	C_3H_6	This work
4 wt% Ag/Al_2O_3	66.1	61.6	H_2+C_3H_6	This work
	80.3	122.8	C_3H_6	This work
6 wt% Ag/Al_2O_3	60.4	55.6	H_2+C_3H_6	This work
2 wt% Ag/Al_2O_3	61		H_2+C_3H_8	[13]
	224		C_3H_8	[13]
2.2 wt% Ag/Al_2O_3	26		H_2+C_3H_6	[31]
	105		C_3H_6	[31]

Table 3
Reaction orders for NOx conversion over Ag/Al_2O_3.

	H_2-C_3H_6-SCR		H_2O-H_2-C_3H_6-SCR	
	2 wt% Ag/Al_2O_3	4 wt% Ag/Al_2O_3	2 wt% Ag/Al_2O_3	4 wt% Ag/Al_2O_3
Order in NO[a]	0.56	0.72	0.40	0.65
Order in C_3H_6[b]	−0.62	0.56	0.73	0.73

[a] NO concentration range is 200 ppm to 1000 ppm.
[b] C_3H_6 concentration range is 800 ppm to 2000 ppm.

vapor slightly decreased the reaction order of NO to 0.40. As for the 4 wt% Ag/Al_2O_3, the effect of water vapor on the NO reaction order was marginal, giving the value of 0.72 under water-free conditions and 0.65 in the presence of moisture. As shown in Fig. 6B, surprisingly, the addition of water vapor increased the C_3H_6 reaction order from a negative value (−0.62) to a positive value (0.73) over 2 wt%

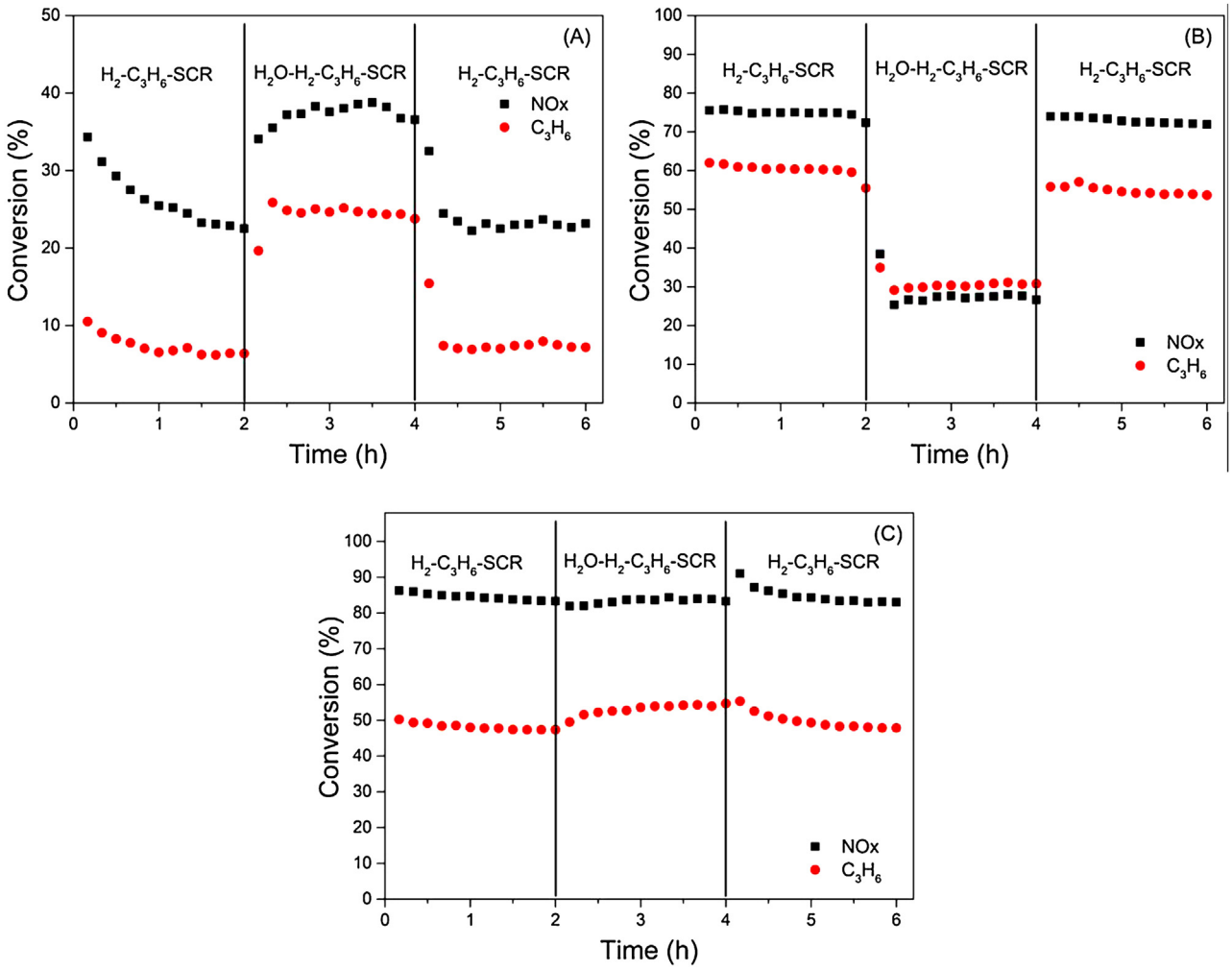

Fig. 4. Step-response experiment over (A) 2 wt% Ag/Al_2O_3 at a GHSV = 100,000 (weight of catalyst = 0.3 g), (B) 4 wt% Ag/Al_2O_3 at a GHSV = 300,000 (weight of catalyst = 0.1 g) at 265 °C, and (C) 2 wt% Ag/Al_2O_3 at a GHSV = 300,000 (weight of catalyst = 0.1 g) at 400 °C in the fixed-bed reactor. Feed composition: NO 800 ppm, C_3H_6 1714 ppm, H_2 1%, O_2 10%, H_2O 10% (when added), N_2 balance.

Ag/Al_2O_3. This result indicates that under water-free conditions, the reaction rate for NOx conversion decreased with increasing C_3H_6 concentration, while this apparent poisoning effect was overcome by the introduction of water vapor, further confirming the enhancement effect of water vapor on NOx conversion (Fig. 2B) and C_3H_6 conversion (Fig. 3B). Over 4 wt% Ag/Al_2O_3, however, the reaction order of C_3H_6 was slightly increased by the addition of water vapor (from 0.56 to 0.73), indicating that the surface reaction involved in C_3H_6 oxidation was retarded by water vapor, which was also in agreement with the results of activity testing (Fig. 3C).

The results of kinetic studies show that the introduction of water vapor does not change the apparent activation energy of NOx reduction in H_2-assisted C_3H_6-SCR, indicating that the reaction pathway for NOx reduction remains the same over 2 wt% and 4 wt% Ag/Al_2O_3. Over the two catalysts, however, the effect of water vapor on the C_3H_6 reaction order was distinctly different. This result possibly suggests that the adsorption and activation of C_3H_6 are closely related to water vapor. To highlight this issue, further *in situ* DRIFTS measurements were performed, as presented in the next section.

3.4. In situ *DRIFTS studies for NOx reduction by* C_3H_6

3.4.1. *Influence of* H_2O *on the partial oxidation of* C_3H_6

Generally, the process of HC-SCR over Ag/Al_2O_3 begins with the partial oxidation of hydrocarbons to produce reactive species [1,15,21,56]. Therefore, the *in situ* DRIFTS of 2 wt% Ag/Al_2O_3 during exposure to H_2+C_3H_6+O_2 was measured first, with the results shown in Fig. 7. In this case, characteristic peaks due to surface species originating from the partial oxidation of C_3H_6 were observed at the temperature of 150 °C (Fig. 7A). The peaks at 1591, 1394, and 1375 cm^{-1} are assigned to adsorbed formate [20]. The appearance of peaks at 1576 and 1458 cm^{-1} indicates the formation of adsorbed acetates [18,22,29,57]. According to previous research works [35,41,58,59], the shoulder peak appearing at 1633 cm^{-1} can be attributed to adsorbed enolic species. Keeping the structural features of surface enolates (C═C—O^-) in mind, there should be two other characteristic vibration frequencies, located at around 1416 and 1336 cm^{-1}. However, the low concentration of enolic species derived from the partial oxidation of C_3H_6 might explain the absence of the two peaks. In addition, a shoulder peak at 1669 cm^{-1} assignable to adsorbed acetone was observed over Ag/Al_2O_3 [20,60].

If the reaction time is taken into account, one can easily find that formate was preferentially formed or was stable on the surface of catalysts: 1) it appeared first in the initial stage of partial oxidation of C_3H_6; and 2) the high-frequency peak (1591 cm^{-1}) assignable to formate species always exhibited the strongest intensity. It was only after 50 min of exposure to H_2+C_3H_6+O_2 that the characteristic peak (1633 cm^{-1}) of enolic species appeared, indicative of its instability.

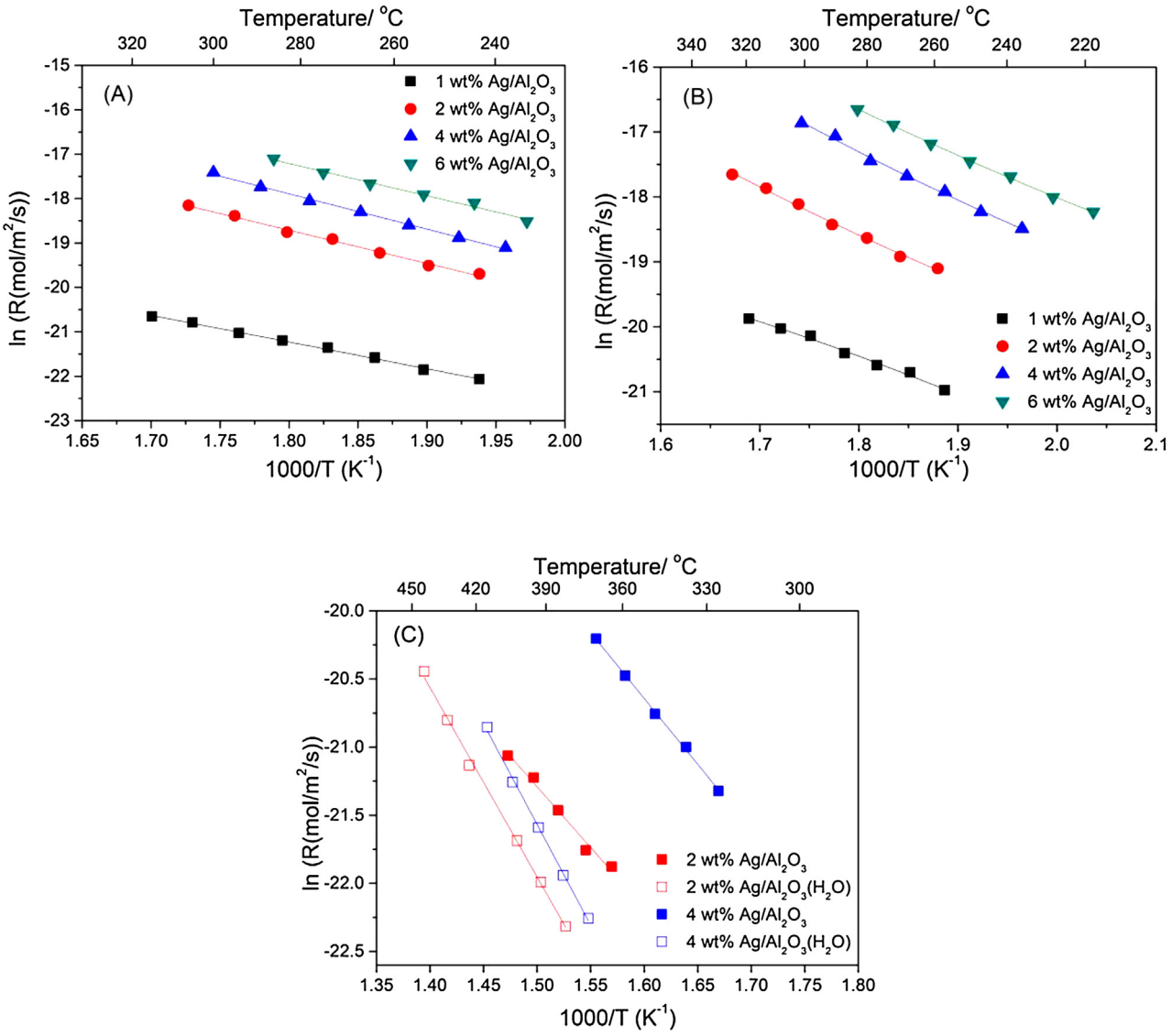

Fig. 5. Arrhenius plots for the rate of NOx conversion over Ag/Al_2O_3 catalysts in different conditions (A) H_2-C_3H_6-SCR without water vapor, (B) H_2-C_3H_6-SCR with water vapor, and (C) C_3H_6-SCR with or without water vapor. Feed composition: 800 ppm NO, 1714 ppm C_3H_6, 10% O_2, 1% H_2 (when added), 10% H_2O (when added), and N_2 balance. GHSV: varying in the range of 100,000–3,000,000 h^{-1} in order to obtain NOx conversion below 20%.

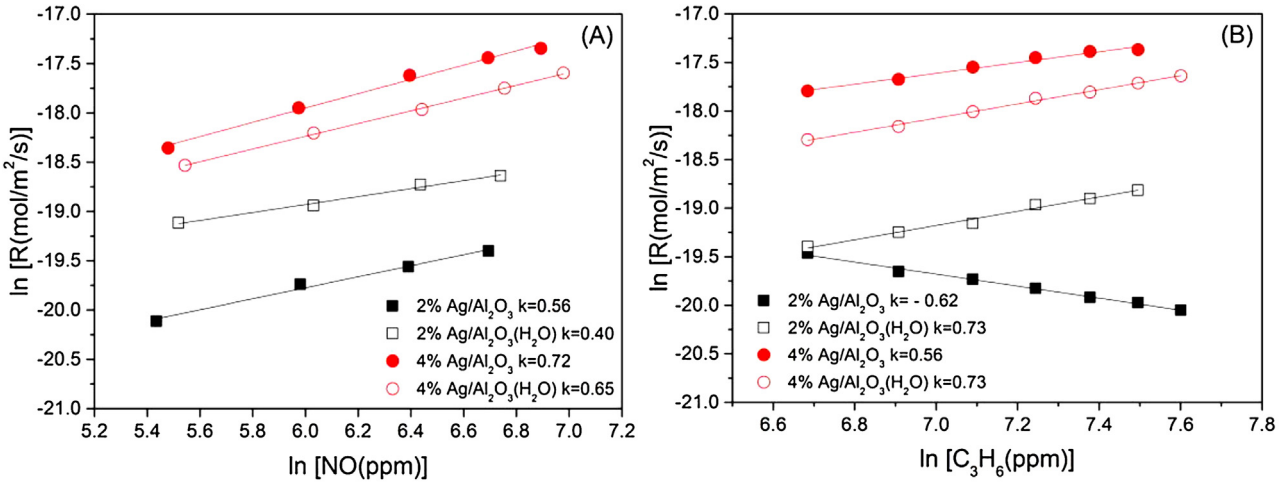

Fig. 6. Reaction rates of NOx conversion as a function of (A) NO and (B) C_3H_6 concentration over Ag/Al_2O_3 at 280 °C.

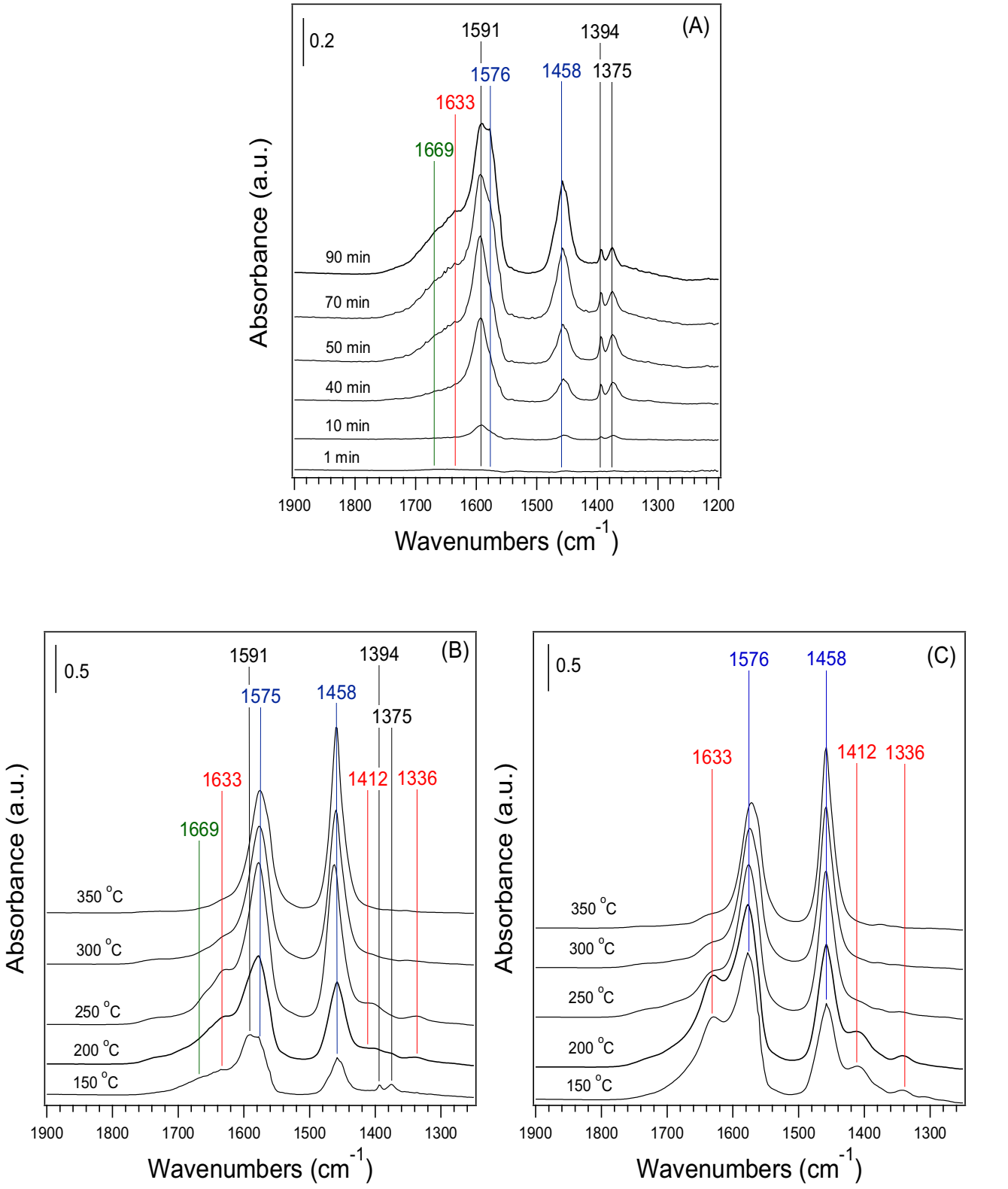

Fig. 7. Dynamic change of *in situ* DRIFTS spectra of adsorbed species on 2 wt% Ag/Al_2O_3 during the oxidation of C_3H_6 in the presence of H_2 at 150 °C (A). *In situ* DRIFTS spectra of adsorbed species on (B) 2 wt% Ag/Al_2O_3 and (C) 4 wt% Ag/Al_2O_3 in steady states in a flow of $C_3H_6 + H_2 + O_2$ at different temperatures. Feed composition: C_3H_6 1714 ppm, H_2 1%, O_2 10%, N_2 balance.

Under the same gas feed conditions, the *in situ* DRIFTS spectra of 2 wt% Ag/Al_2O_3 was further measured at elevated temperatures (Fig. 7B). As temperature increased, the intensities of peaks due to formate significantly decreased, and disappeared at temperatures above 250 °C. In contrast, the intensity of peaks due to acetate species distinctly increased, becoming predominant at temperatures above 250 °C. The peak at 1633 cm^{-1} increased in intensity as temperature increased from 150 °C to 250 °C, indicating an increase

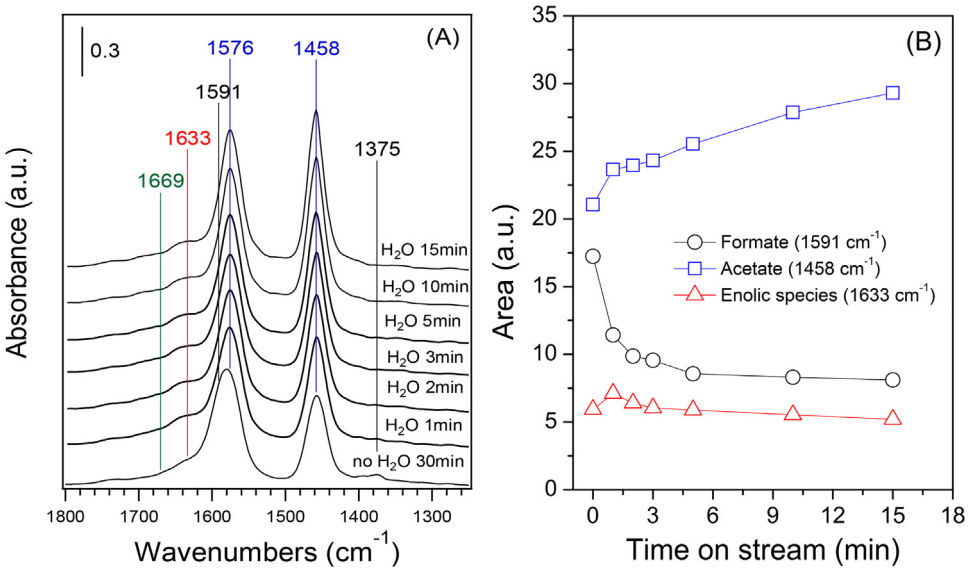

Fig. 8. Dynamic changes of *in situ* DRIFTS spectra of adsorbed species over 2 wt% Ag/Al_2O_3 as a function of time in a flow of $H_2O + H_2 + C_3H_6 + O_2$ at 265 °C (A), and (B) the integrated areas of the peaks due to formate (1591 cm^{-1}), acetate (1458 cm^{-1}), and enolic species (1633 cm^{-1}) in the case of (A). Before measurement, the catalyst was pre-exposed to a flow of $H_2 + C_3H_6 + O_2$ for 30 min at 265 °C. Feed composition: C_3H_6 1714 ppm, H_2 1%, O_2 10%, H_2O 5% (when added), N_2 balance.

in the concentration of surface enolic species. This increase was accompanied by the appearance of low-frequency bands at 1412 and 1336 cm^{-1} due to the enolic species. Raising the reaction temperature further lowered the concentration of enolic species over 2 wt% Ag/Al_2O_3.

The same set of DRIFTS measurements was also carried out over 4 wt% Ag/Al_2O_3, with the results shown in Fig. 7C. Notably, the characteristic peaks assignable to formate were hardly observed, while those of acetate (1576 and 1458 cm^{-1}) were predominant over the whole temperature range. Characteristic frequencies of enolic species were clearly observed at 1633, 1412, and 1336 cm^{-1} at temperatures between 150 °C and 200 °C. Within this temperature range, meanwhile, the highest-frequency peak of the enolic species exhibited much stronger intensity compared with the results presented in Fig. 7B.

The effect of moisture content on the partial oxidation of C_3H_6 over 2 wt% Ag/Al_2O_3 was further studied by *in situ* DRIFTS at 265 °C (Fig. 8A). In order to clarify the dynamic change of surface intermediates induced by the introduction of water vapor, the spectra (Fig. 8A) in the range of 1200–1800 cm^{-1} were then fitted and deconvoluted to the constituent peaks (with typical results presented in Fig. S7). The integrated areas of peaks at 1591 cm^{-1} (for formate), 1458 cm^{-1} (for acetate), and 1633 cm^{-1} (for enolic species) are plotted as a function of time-on-stream (Fig. 8B). As can be seen from Fig. 8A, after exposure of 2 wt% Ag/Al_2O_3 to a gas mixture of $H_2 + C_3H_6 + O_2$ for 30 min, strong peaks due to formate (1591 cm^{-1}) and acetate (1458 and 1576 cm^{-1}) were observed, along with the generation of enolic species (1633 cm^{-1}). The addition of water vapor significantly decreased the intensity of the peaks due to formate in the first 2 min, followed by more gradual decrease (Fig. 8B). As the concentration of formate decreased, the intensity of enolic species was slightly increased in the initial 1 min of water introduction, and then decreased slowly. During the entire process of water addition, meanwhile, a monotonic increase in the intensity of acetate was observed over 2 wt% Ag/Al_2O_3.

3.4.2. *Influence of H_2O on H_2-C_3H_6-SCR over Ag/Al_2O_3*

Over the 2 wt% Ag/Al_2O_3, the kinetic study (Fig. 6 and Table 3) showed that the reaction order of C_3H_6 for H_2-C_3H_6-SCR was −0.62, indicating that certain products derived from C_3H_6 partial oxidation inhibited the reduction of NOx. To highlight this issue, an *in situ* DRIFTS experiment was carried out under H_2-C_3H_6-SCR conditions while increasing the concentration of C_3H_6 from 429 ppm to 1714 ppm (Fig. 9). As the C_3H_6 concentration increased, notably, the intensities of the peaks due to formate (1591, 1392, and 1375 cm^{-1}) distinctly increased, indicating that the formate coverage strongly depended on the C_3H_6 concentration. During this process, increased intensities of peaks assignable to acetate (1458 cm^{-1}) and enolic species (1633 cm^{-1}) were also observed, while their intensities, particularly for the acetate, were

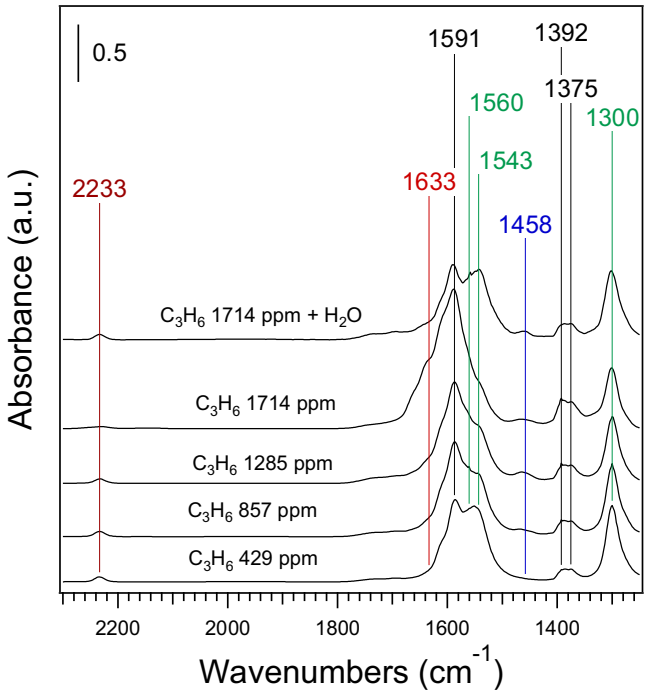

Fig. 9. DRIFTS spectra of adsorbed species during H_2-C_3H_6-SCR with varying C_3H_6 concentration over 2 wt% Ag/Al_2O_3 at steady state at 265 °C. Feed composition: NO 800 ppm, C_3H_6 from 429 to 1714 ppm, H_2 1%, O_2 10%, H_2O 5% (when added), N_2 balance.

much lower than that of formate. Also, —NCO (2233 cm^{-1}), monodentate nitrate (1560–1543 cm^{-1}), and isolated bidentate nitrate (1300 cm^{-1}) were observed [2,15,61]. It has been widely accepted that the —NCO species, derived from the reaction between adsorbed nitrates and oxygenated HC species (including enolic species and acetate), is a key intermediate in the HC-SCR of NOx over Ag/Al_2O_3 [1,2,62]. The —NCO species shows high reactivity toward $NO+O_2$ to produce N_2, the appearance of which thus indicates that the global NOx reduction process has occurred. An increased intensity of —NCO species was observed after water vapor was introduced into the gas mixture, indicative of the enhancement for NOx reduction, which was in agreement with the activity result (Fig. 4).

Over Ag/Al_2O_3, our previous study [20] showed that C_3H_6 was more efficient for NOx reduction than CH_4. Formate, as the main product of partial oxidation of CH_4, exhibited low reactivity toward $NO + O_2$ to produce —NCO, finally leading to a low deNOx activity for CH_4 over Ag/Al_2O_3. The acetate and enolic species exhibit higher activity, thus playing an important role in C_3H_6-SCR and H_2-C_3H_6-SCR, respectively [20]. With this in mind, it is clear that formate acts as a spectator in H_2-C_3H_6-SCR, accumulating severely on the reaction sites of 2 wt% Ag/Al_2O_3 and inhibiting the adsorption and subsequent activation of other reactants, thus contributing to a negative reaction order of C_3H_6 for NOx reduction. Addition of water vapor significantly decreased the formate coverage on the surface of the silver catalyst, giving more sites available for other active intermediates, and thus increased SCR activity. Similarly, a negative reaction order of NO (−2.53) for C_3H_8-SCR was observed by Shimizu et al. [13], the occurrence of which was induced by nitrate coverage on the surface of Ag/Al_2O_3. Further research indicated that addition of hydrogen was effective in decreasing nitrate coverage, leading to a positive value of NO reaction order (0.49).

As shown in Fig. 8A, formate, acetate and enolic species adsorbed on the surface of 2 wt% Ag/Al_2O_3 were produced by the partial oxidation of C_3H_6. The produced enolic species and acetate exhibit high activity towards $NO+O_2$, leaving the inert formate on the surface of the silver catalyst. As a result, formate was predominant during the H_2-C_3H_6-SCR process (Fig. 9). Introduction of water vapor into $H_2 + C_3H_6 + O_2$ enhanced the generation of enolic species and acetate (Fig. 8A and B). The enolic species was clearly observed during H_2-C_3H_6-SCR over 2 wt% Ag/Al_2O_3, while the acetate exhibited a low concentration (Fig. 9). Introduction of water vapor into the gas feed of H_2-C_3H_6-SCR significantly decreased the intensity of enolic species, whereas it hardly changed the surface concentration of acetate. During the H_2-C_3H_6-SCR over 2 wt% Ag/Al_2O_3, activity measurement showed that water vapor introduction promoted NOx and C_3H_6 conversion (Fig. 4A). As a result, it can be concluded that the decrease of enolic species concentration induced by the introduction of water vapor into the H_2-C_3H_6-SCR system was derived from accelerated consumption of enolic species. This result, in turn, suggests that the pathway involving the generation of enolic species and its further transformation plays a crucial role in the H_2-C_3H_6-SCR process over 2 wt% Ag/Al_2O_3, particularly at low temperatures.

3.5. DFT calculations

Kinetic studies and *in situ* DRIFTS measurements confirmed that water vapor significantly changed the behaviors of surface formate, acetate, and enolic species, thus contributing to the activity of 2 wt% Ag/Al_2O_3 for H_2-C_3H_6-SCR. To highlight this issue, the adsorption of these species on a Ag/Al_2O_3 slab and hydroxylated Ag/Al_2O_3 slab was calculated. Over this catalyst, UV–vis spectra clearly showed that the silver cations were predominant. According to our previous NMR and DFT calculations, silver ions over 2 wt% Ag/Al_2O_3 might be bound on tetra- and octa-coordinate Al sites, forming Ag–O–Al_{octa} (on Ag/Al_2O_3 (100) surface) and Ag–O–Al_{tetra} (on Ag/Al_2O_3 (110) surface) entities. As a result, periodic models of Ag/Al_2O_3 catalysts and their hydroxylated counterparts containing these two structural features were established (Fig. S2). Over Ag/Al_2O_3, *in situ* DRIFTS and the corresponding calculation results confirmed that the enolic species was preferentially linked with Ag sites, while the acetate tended to adsorb on Al sites [35]. Over pure Al_2O_3, the partial oxidation of C_3H_6 in the presence of H_2 was also measured by *in situ* DRIFTS, with the results shown in Fig. S8. In this case, it should be noted that the formate exhibits the same characteristic frequencies peaks as those on Ag/Al_2O_3, strongly suggesting that the formate is preferentially linked with Al sites. Keeping such intrinsic properties in mind, periodic models for the adsorbed enolic species, acetate, and formate on the Ag/Al_2O_3 surface were established and the relaxed structures are shown in Figs. S9–S11, respectively.

The DFT-calculated adsorption energies are summarized in Table 4. All of the adsorption energies had negative values, which indicates that the surface has a strong affinity for the formate, acetate, and enolic species. For the dehydrated Ag/Al_2O_3 surface, the adsorption energies of formate, acetate, and enolic species on the Ag/Al_2O_3 (110) surface are more negative than on the Ag/Al_2O_3 (100) surface, which indicates that these species are preferentially adsorbed on the (110) surface. Previous theoretical calculations and experimental results showed that the (110) surface predominates on γ-Al_2O_3, with about 70% of the total area, followed by the (100) surface (~20%) [63,64]. The adsorption energies of formate (−2.84 eV) and acetate (−3.09 eV) were significantly more negative than that of the enolic species (−1.99 eV), meaning that formate and acetate are more easily formed on the (110) surface, which is consistent with the results of DRIFTS.

On the hydroxylated Ag/Al_2O_3 (110) surface, the values of adsorption energies for all of the three species became less negative compared to those on the dehydrated Ag/Al_2O_3 surface, meaning the adsorption of these species will be weakened. Such weakening was consistent with a final decreased intensity of IR adsorption bands assignable to the formate and enolic species derived from water vapor addition (Fig. 8). For the acetate species adsorbed on the hydroxylated Ag/Al_2O_3 (110) surface, the 55% weakening of the adsorption energy seems contradictory with the increase of the integrated areas of the IR peak induced by water introduction. On the Ag/Al_2O_3 (100) surface, however, the presence of hydroxyl groups leads to an obvious strengthening (42%) of the adsorption energy of acetate. These results suggest that the adsorption of acetate on the (100) surface is much more favorable than that on the (110) surface in the presence of hydroxyl groups. As a result, it is reasonable that the amount of acetate was increased in the presence of moisture. As can be seen from Table 4, also, the adsorption energy for formate on the (100) surface is more negative in the presence of hydroxyl, whereas the adsorption of formate (−3.70 eV) is still weaker than that of acetate (−3.84 eV). This means that the adsorption of formate is more difficult on the (100) surface considering its competitive adsorption with acetate for the same Al sites.

During the partial oxidation of C_3H_6 over 2 wt% Ag/Al_2O_3 (Fig. 8), it should be noted that an increased intensity of enolic species was clearly observed in the initial stage of water introduction, followed by a slow decrease. After 5 min of water addition, the concentration of enolic species was lower than that under water-free condition. Such dynamic behavior of enolic species triggered by water vapor addition can be explained as follows. As shown in Fig. S8 and S10, although the enolic species and formate were adsorbed on different sites (the enolic species was bound on Ag sites while the formate adsorbed on Al sites), a high concentration of formate would result in a strong steric effect on the adsorption of enolic species. This steric effect would occur during the partial oxidation of C_3H_6 without water vapor. Introduction of water vapor

Table 4
DFT-calculated adsorption energies.

Model	adsorption energy (eV)		
	$HCOO^-$	$CH_2{=}CHO^-$	CH_3COO^-
$Ag/Al_2O_3(110)$	−2.84	−1.99	−3.09
$20OH\text{-}Ag/Al_2O_3(110)$	−1.62 (−43%)	−1.40 (−30%)	−1.39 (−55%)
$Ag/Al_2O_3(100)$	−2.78	−1.95	−2.71
$12OH\text{-}Ag/Al_2O_3(100)$	−3.70 (33%)	−1.86 (−4%)	−3.84 (42%)

The number in brackets is the change percentage.

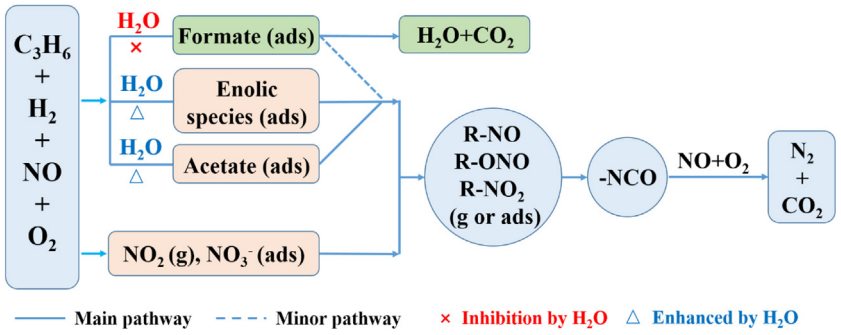

Scheme 1. Proposed interpretation of water influence on the H_2 assisted C_3H_6-SCR over Ag/Al_2O_3.

significantly decreased the concentration of formate over Ag/Al_2O_3, reducing the steric effect and enabling more silver sites to be available for enolic species. As a result, an increased intensity of enolic species appeared in the initial stage of water introduction. On the other hand, water vapor addition induced hydroxylation of the Ag/Al_2O_3 surface, the occurrence of which decreases the adsorption energy of enolic species. Thus, it is reasonable that the concentration of surface enolic species in the final stage of water vapor addition was lower than that under water-free conditions.

4. Discussion

Over the 4 wt% Ag/Al_2O_3 catalyst, DRIFTS and GC–MS measurements revealed that the enolic species produced by the partial oxidation of C_3H_6 in the presence of H_2 showed high activity for reaction with $NO+O_2$ to form N_2, which can be considered to occur as follows: $C_3H_6 + H_2 + NO + O_2 \rightarrow$ ad-NOx + enolic species (acetate also formed) $\rightarrow R{-}ONO + R{-}NO_2 \rightarrow {-}NCO + {-}CN \rightarrow N_2$ [15,20]. During this process, acetate was also produced, which exhibited a lower activity than enolic species; thus the pathway involving the generation of enolic species and their further reaction governs the H_2-C_3H_6-SCR process, particularly in the low temperature region. Over 2 wt% Ag/Al_2O_3, the kinetic studies presented here show that the apparent activation energy for NOx reduction was almost the same as that obtained with 4 wt% Ag/Al_2O_3, indicative of a similar pathway of NOx reduction (Scheme 1). Over 2 wt% Ag/Al_2O_3, formate also formed during the partial oxidation of C_3H_6, while this species exhibited low activity toward $NO+O_2$. During H_2-C_3H_6-SCR, the produced enolic species and acetate were consumed by reaction with $NO+O_2$ (and/or surface nitrates), while the formate tended to accumulate seriously, thus exhibiting a poisoning effect on the reduction of NOx over 2 wt% Ag/Al_2O_3. The introduction of water vapor into the H_2-C_3H_6-SCR system decreased the formate coverage, leaving more sites for the generation of active species (including enolic species and acetates) and also for their further reaction. As a result, the NOx reduction was promoted by water vapor addition over 2 wt% Ag/Al_2O_3, which was confirmed by the kinetic studies and *in situ* DRIFTS measurements.

UV–vis analysis revealed that silver cations (Ag^+), oxidized silver clusters ($Ag_n^{\delta+}$), and metallic silver clusters (Ag_n^0) were present on the surface of Ag/Al_2O_3. As for the process of HC-SCR taking place over Ag/Al_2O_3, the oxidized silver species (Ag^+ and $Ag_n^{\delta+}$) contributed to partial oxidation of the reductant, thus serving as the active sites for NOx reduction. The metallic silver entities were often present on Ag/Al_2O_3 with high silver content, promoting the complete oxidation of reductant to produce CO_2 [1,2,33,37]. As for 2 wt% Ag/Al_2O_3, oxidized silver species were predominant while the metallic entities exhibited a low proportion, thus the transformation of formate to CO_2 was difficult at low temperatures during the H_2-C_3H_6-SCR. An increase in metallic silver clusters was clearly observed over 4 wt% Ag/Al_2O_3. This means that the 4 wt% Ag/Al_2O_3 had stronger oxidizing ability than the catalyst with 2 wt% Ag loading, accelerating the decomposition of formate so that this inert species was hardly observed over the whole temperature region in the process of NOx reduction.

Water adsorption is inevitable on oxide surfaces, serving as a promoter/reactant or as an inhibitor in a given reaction taking place over oxide surfaces. Just by tuning the loading of silver, interestingly, quite opposite effects of water vapor were clearly observed over Ag/Al_2O_3 catalysts for H_2-C_3H_6-SCR. As for the water-gas shift reaction, molecular water would react with the key intermediate of surface formate to produce CO_2 and H_2 [65], which is quite different from our result. The theoretical calculation presented here shows that the presence of water can weaken the interactions between the Ag/Al_2O_3 surface and the spectator species formate, thus more surface sites become available for the formation of active intermediates such as acetate.

Over Ag/Al_2O_3 catalysts, it has been suggested that the addition of H_2 enhanced activation of O_2 to active oxygen species (*e.g.* O_2^- and OOH species), and then benefited the partial oxidation of hydrocarbons and NOx reduction [21,66]. In our case, it is possible that the active oxygen species mentioned above would be produced during the H_2-C_3H_6-SCR. On an oxide surface such as the Al_2O_3 surface, meanwhile, dissociative adsorption of H_2O molecules often occurs, providing an efficient pathway for the regeneration of active oxygen species [40]. With this in mind, the presence of water vapor also gives the possibility for the promotion of the H_2-C_3H_6-SCR process, by regeneration of active oxygen species produced by O_2 activation.

5. Conclusion

Oxidized silver species contributed to the partial oxidation of C_3H_6, also serving as the active sites for H_2-assisted C_3H_6-SCR over Ag/Al_2O_3, while metallic silver clusters exhibited strong oxidizing properties and thus promoted the complete oxidation of the reductant to produce CO_2. Over 2 wt% Ag/Al_2O_3, oxidized silver species were predominant, with a small fraction of metallic silver. As a result, the 2 wt% Ag/Al_2O_3 was highly active for H_2-C_3H_6-SCR, whereas it was inactive for the low-temperature transformation of inert formate to CO_2 in the absence of water vapor. In this case, a serious accumulation of formate thus induced a poisoning effect for NOx conversion over 2 wt% Ag/Al_2O_3, the occurrence of which was confirmed by *in situ* DRIFTS and kinetic studies. *In situ* DRIFTS and DFT calculation studies further revealed that the water molecule may serve as a scavenger of inert formate; its addition therefore significantly decreased the formate coverage, giving more surface sites available for the generation of active enolic species and acetates, finally leading to an increase in the low-temperature activity of 2 wt% Ag/Al_2O_3 for H_2-C_3H_6-SCR.

Acknowledgment

This work was supported by the National Natural Science Foundation of China (21373261, 21673277, and 21637005).

Appendix A. Supplementary data

Supplementary data associated with this article can be found, in the online version, at http://dx.doi.org/10.1016/j.apcatb.2017.02.001.

References

[1] R. Burch, J.P. Breen, F.C. Meunier, Appl. Catal. B-Environ. 39 (2002) 283–303.
[2] H. He, Y.B. Yu, Catal. Today 100 (2005) 37–47.
[3] P. Granger, V.I. Parvulescu, Chem. Rev. 111 (2011) 3155–3207.
[4] M.K. Kim, P.S. Kim, J.H. Baik, I.S. Nam, B.K. Cho, S.H. Oh, Appl. Catal. B-Environ. 105 (2011) 1–14.
[5] K. Shimizu, A. Satsuma, Phys. Chem. Chem. Phys. 8 (2006) 2677–2695.
[6] Z.M. Liu, S.I. Woo, Catal. Rev. 48 (2006) 43–89.
[7] Z.M. Liu, J.H. Li, A.S.M. Junaid, Catal. Today 153 (2010) 95–102.
[8] R. Burch, Catal. Rev. 46 (2004) 271–333.
[9] J.H. Li, R. Ke, W. Li, J.M. Hao, Catal. Today 126 (2007) 272–278.
[10] F. Gunnarsson, J.A. Pihl, T.J. Toops, M. Skoglundh, H. Harelind, Appl. Catal. B-Environ. 202 (2017) 42–50.
[11] S. Satokawa, Chem. Lett. (2000) 294–295.
[12] S. Satokawa, J. Shibata, K. Shimizu, S. Atsushi, T. Hattori, Appl. Catal. B-Environ. 42 (2003) 179–186.
[13] K. Shimizu, J. Shibata, A. Satsuma, J. Catal. 239 (2006) 402–409.
[14] S. Satokawa, J. Shibata, K.I. Shimizu, A. Satsuma, T. Hattori, T. Kojima, Chem. Eng. Sci. 62 (2007) 5335–5337.
[15] X.L. Zhang, Y.B. Yu, H. He, Appl. Catal. B-Environ. 76 (2007) 241–247.
[16] C. Thomas, Appl. Catal. B-Environ. 162 (2015) 454–462.
[17] L. Strom, P.A. Carlsson, M. Skoglundh, H. Harelind, Appl. Catal. B-Environ. 181 (2016) 403–412.
[18] P. Sazama, L. Capek, H. Drobna, Z. Sobalik, J. Dedecek, K. Arve, B. Wichterlova, J. Catal. 232 (2005) 302–317.
[19] R. Brosius, K. Arve, M.H. Groothaert, J.A. Martens, J. Catal. 231 (2005) 344–353.
[20] Y.B. Yu, H. He, X.L. Zhang, H. Deng, Catal. Sci. Technol. 4 (2014) 1239–1245.
[21] K. Shimizu, K. Sawabe, A. Satsuma, Catal. Sci. Technol. 1 (2011) 331–341.
[22] J. Shibata, K. Shimizu, S. Satokawa, A. Satsuma, T. Hattori, Phys. Chem. Chem. Phys. 5 (2003) 2154–2160.
[23] U. Bentrup, M. Richter, R. Fricke, Appl. Catal. B-Environ. 55 (2005) 213–220.
[24] K. Shimizu, A. Satsuma, T. Hattori, Appl. Catal. B-Environ. 25 (2000) 239–247.
[25] F.C. Meunier, R. Ukropec, C. Stapleton, J.R.H. Ross, Appl. Catal. B-Environ. 30 (2001) 163–172.
[26] A. Shichi, T. Hattori, A. Satsuma, Appl. Catal. B-Environ. 77 (2007) 92–99.
[27] M. Richter, U. Bentrup, R. Eckelt, M. Schneider, M.M. Pohl, R. Fricke, Appl. Catal. B-Environ. 51 (2004) 261–274.
[28] T. Miyadera, Appl. Catal. B-Environ. 2 (1993) 199–205.
[29] K. Shimizu, J. Shibata, H. Yoshida, A. Satsuma, T. Hattori, Appl. Catal. B-Environ. 30 (2001) 151–162.
[30] T. Chaieb, L. Delannoy, C. Louis, C. Thomas, Appl. Catal. B-Environ. 142 (2013) 780–784.
[31] T. Chaieb, L. Delannoy, G. Costentin, C. Louis, S. Casale, R.L. Chantry, Z.Y. Li, C. Thomas, Appl. Catal. B-Environ. 156 (2014) 192–201.
[32] N.A. Sadokhina, A.F. Prokhorova, R.I. Kvon, I.S. Mashkovskii, G.O. Bragina, G.N. Baeva, V.I. Bukhtiyarov, A.Y. Stakheev, Kinet. Catal. 53 (2012) 107–116.
[33] K. Shimizu, M. Tsuzuki, K. Kato, S. Yokota, K. Okumura, A. Satsuma, J. Phys. Chem. C 111 (2007) 950–959.
[34] H. Deng, Y.B. Yu, F.D. Liu, J.Z. Ma, Y. Zhang, H. He, ACS Catal. 4 (2014) 2776–2784.
[35] Y. Yan, Y.B. Yu, H. He, J.J. Zhao, J. Catal. 293 (2012) 13–26.
[36] Y.B. Yu, J.J. Zhao, Y. Yan, X. Han, H. He, Appl. Catal. B-Environ. 136 (2013) 103–111.
[37] X. She, M. Flytzani-Stephanopoulos, J. Catal. 237 (2006) 79–93.
[38] H. Deng, Y.B. Yu, H. He, Chin. J. Catal. 36 (2015) 1312–1320.
[39] H. Deng, Y.B. Yu, H. He, J. Phys. Chem. C 119 (2015) 3132–3142.
[40] M. Digne, P. Sautet, P. Raybaud, P. Euzen, H. Toulhoat, J. Catal. 211 (2002) 1–5.
[41] P.S. Kim, M.K. Kim, B.K. Cho, I.S. Nam, S.H. Oh, J. Catal. 301 (2013) 65–76.
[42] B. Wichterlova, P. Sazama, J.P. Breen, R. Burch, C.J. Hill, L. Capek, Z. Sobalik, J. Catal. 235 (2005) 195–200.
[43] G.D.-M.M. Boudart, Kinetics of Heterogeneous Catalytic Reactions, Princeton University Press, Princeton, NJ, 1984.
[44] S. Tamm, L. Olsson, S. Fogel, P. Gabrielsson, M. Skoglundh, AIChE J. 59 (2013) 4325–4333.
[45] B. Sawatmongkhon, A. Tsolakis, K. Theinnoi, A.P.E. York, P.J. Millington, R.R. Rajaram, Appl. Catal. B-Environ. 111 (2012) 165–177.
[46] W.L. Johnson, G.B. Fisher, T.J. Toops, Catal. Today 184 (2012) 166–177.
[47] S. Chansai, R. Burch, C. Hardacre, J. Breen, F. Meunier, J. Catal. 281 (2011) 98–105.
[48] A.B. Mhadeshwar, B.H. Winkler, B. Eiteneer, D. Hancu, Appl. Catal. B-Environ. 89 (2009) 229–238.
[49] D. Creaser, H. Kannisto, J. Sjoblom, H.H. Ingelsten, Appl. Catal. B-Environ. 90 (2009) 18–28.
[50] J.R.H. Carucci, A. Kurman, H. Karhu, K. Arve, K. Eranen, J. Warna, T. Salmi, D.Y. Murzin, Chem. Eng. J. 154 (2009) 34–44.
[51] K. Arve, J.R.H. Carucci, K. Eranen, A. Aho, D.Y. Murzin, Appl. Catal. B-Environ. 90 (2009) 603–612.
[52] J.P. Breen, R. Burch, C. Hardacre, C.J. Hill, C. Rioche, J. Catal. 246 (2007) 1–9.
[53] K. Arve, F. Klingstedt, K. Eranen, J. Warna, L.E. Lindfors, D.Y. Murzin, Chem. Eng. J. 107 (2005) 215–220.
[54] K. Eranen, L.E. Lindfors, F. Klingstedt, D.Y. Murzin, J. Catal. 219 (2003) 25–40.
[55] M. Haneda, Y. Kintaichi, H. Shimada, H. Hamada, J. Catal. 192 (2000) 137–148.
[56] J.H. Li, R. Ke, W. Li, J.M. Hao, Catal. Today 139 (2008) 49–58.
[57] F.C. Meunier, J.P. Breen, V. Zuzaniuk, M. Olsson, J.R.H. Ross, J. Catal. 187 (1999) 493–505.
[58] Y.B. Yu, H. He, Q.C. Feng, H.W. Gao, X. Yang, Appl. Catal. B-Environ. 49 (2004) 159–171.
[59] Y.B. Yu, X.P. Song, H. He, J. Catal. 271 (2010) 343–350.
[60] M.I. Zaki, M.A. Hasan, L. Pasupulety, Langmuir 17 (2001) 768–774.
[61] X.L. Zhang, H. He, H.W. Gao, Y.B. Yu, Spectrochim. Acta. A 71 (2008) 1446–1451.
[62] K. Shimizu, J. Shibata, A. Satsuma, T. Hattori, Phys. Chem. Chem. Phys. 3 (2001) 880–884.
[63] M. Digne, P. Sautet, P. Raybaud, P. Euzen, H. Toulhoat, J. Catal. 226 (2004) 54–68.
[64] P. Nortier, P. Fourre, A.B.M. Saad, O. Saur, J.C. Lavalley, Appl. Catal. 61 (1990) 141–160.
[65] J. Paier, C. Penschke, J. Sauer, Chem. Rev. 113 (2013) 3949–3985.
[66] K. Shimizu, A. Satsuma, J. Phys. Chem. C 111 (2007) 2259–2264.